Supplementary Information for *FaIRv2.0.0: a generalised impulse-response model for climate uncertainty and future scenario exploration*

Nicholas J. Leach[1], Stuart Jenkins[1], Zebedee Nicholls[2,3], Christopher J. Smith[4,5], John Lynch[1], Michelle Cain[1], Tristram Walsh[1], Bill Wu[1], Junichi Tsutsui[6], and Myles R. Allen[1,7]

[1]Department of Physics, Atmospheric, Oceanic, and Planetary Physics, University of Oxford, United Kingdom.
[2]Australian–German Climate and Energy College, University of Melbourne, Australia.
[3]School of Geography, Earth and Atmospheric Sciences, University of Melbourne, Australia.
[4]School of Earth and Environment, University of Leeds, Leeds, UK.
[5]International Institute for Applied Systems Analysis, Laxenburg, Austria.
[6]Environmental Science Research Laboratory, Central Research Institute of Electric Power Industry, Abiko, Japan.
[7]Environmental Change Institute, University of Oxford, Oxford, UK.

Correspondence: Nicholas J. Leach (nicholas.leach@stx.ox.ac.uk)

Table S1. Units used in FaIRv2.0.0-alpha when the default parameter set is used for each gas or aerosol species. Default forcing unit for all species is Wm^{-2}.

Variable	CO_2	CH_4	N_2O	SOx	NOx	BC	OC	NH3	VOC	All other WMGHGs
Emissions	PgC	$TgCH_4$	TgN	$TgSO_2$	TgN	TgC	TgC	Tg	Tg	Tg
Concentrations	ppm	ppb	ppb	-	-	-	-	-	-	ppb

S1 FaIRv2.0.0 parameter defaults

Table S2. FaIRv2.0.0 default parameter values. Available to download as a CSV here.

parameter	a_1	a_2	a_3	a_4	τ_1	τ_2	τ_3	τ_4	r_0	r_u	r_T	r_a	PI_conc	emis2conc	f_1	f_2	f_3
bc	1.0	0	0	0	1.0	1.0	1.0	1.0	1.0	0	0	0	1e-15	1.0	0	0.0567	0
bc|aci	-	-	-	-	-	-	-	-	-	-	-	-	-	-	0	-0.00801	0
bc|bc_on_snow	-	-	-	-	-	-	-	-	-	-	-	-	-	-	0	0.0116	0
c2f6	1.0	0	0	0	100.0	1.0	1.0	1.0	185	0	0	0	1e-15	0.0408	0	0.25	0
c3f8	1.0	0	0	0	26.0	1.0	1.0	1.0	133	0	0	0	1e-15	0.0299	0	0.28	0
c4f10	1.0	0	0	0	26.0	1.0	1.0	1.0	133	0	0	0	1e-15	0.0236	0	0.36	0
c5f12	1.0	0	0	0	41.0	1.0	1.0	1.0	170	0	0	0	1e-15	0.0195	0	0.41	0
c6f14	1.0	0	0	0	31.0	1.0	1.0	1.0	149	0	0	0	1e-15	0.0166	0	0.44	0
c7f16	1.0	0	0	0	30.0	1.0	1.0	1.0	146	0	0	0	1e-15	0.0145	0	0.5	0
c8f18	1.0	0	0	0	30.0	1.0	1.0	1.0	146	0	0	0	1e-15	0.0128	0	0.55	0
c_c4f8	1.0	0	0	0	32.0	1.0	1.0	1.0	151	0	0	0	1e-15	0.0281	0	0.32	0
carbon_dioxide	0.217	0.224	0.282	0.276	1000000000	394	36.5	4.3	33.9	0.0188	2.67	0	278	0.469	4.57	0	0.086
carbon_tetrachloride	1.0	0	0	0	0.32	1.0	1.0	1.0	1.79	0	0	0	2.5e-05	0.0366	0	0.174	0
carbon_tetrachloride|o3	-	-	-	-	-	-	-	-	-	-	-	-	-	-	0	-0.255	0
cf4	1.0	0	0	0	500	1.0	1.0	1.0	131	0	0	0	0.034	0.0639	0	0.09	0
cfc11	1.0	0	0	0	0.52	1.0	1.0	1.0	2.91	0	0	0	1e-15	0.041	0	0.26	0
cfc113	1.0	0	0	0	0.93	1.0	1.0	1.0	5.21	0	0	0	1e-15	0.03	0	0.3	0
cfc113|o3	-	-	-	-	-	-	-	-	-	-	-	-	-	-	0	-0.102	0
cfc114	1.0	0	0	0	1.89	1.0	1.0	1.0	10.6	0	0	0	1e-15	0.0329	0	0.31	0
cfc114|o3	-	-	-	-	-	-	-	-	-	-	-	-	-	-	0	-0.0296	0
cfc115	1.0	0	0	0	5.4	1.0	1.0	1.0	30.3	0	0	0	1e-15	0.0364	0	0.2	0
cfc115|o3	-	-	-	-	-	-	-	-	-	-	-	-	-	-	0	-0.00797	0
cfc11|o3	-	-	-	-	-	-	-	-	-	-	-	-	-	-	0	-0.16	0
cfc12	1.0	0	0	0	1.02	1.0	1.0	1.0	5.72	0	0	0	1e-15	0.0465	0	0.32	0
cfc12|o3	-	-	-	-	-	-	-	-	-	-	-	-	-	-	0	-0.0546	0
ch2cl2	1.0	0	0	0	0.00493	1.0	1.0	1.0	0.0276	0	0	0	0.00691	0.0663	0	0.028	0
ch2cl2|o3	-	-	-	-	-	-	-	-	-	-	-	-	-	-	0	0	0
ch3ccl3	1.0	0	0	0	0.05	1.0	1.0	1.0	0.28	0	0	0	1e-15	0.0422	0	0.07	0
ch3ccl3|o3	-	-	-	-	-	-	-	-	-	-	-	-	-	-	0	-0.208	0
chcl3	1.0	0	0	0	0.00501	1.0	1.0	1.0	0.0281	0	0	0	0.006	0.0471	0	0.07	0
chcl3|o3	-	-	-	-	-	-	-	-	-	-	-	-	-	-	0	0	0
co	1.0	0	0	0	1.0	1.0	1.0	1.0	1.0	0	0	0	1e-15	1.0	0	0	0
co|o3	-	-	-	-	-	-	-	-	-	-	-	-	-	-	0	0.000145	0
halon1202	1.0	0	0	0	0.025	1.0	1.0	1.0	0.14	0	0	0	1e-15	0.0268	0	0.27	0
halon1202|o3	-	-	-	-	-	-	-	-	-	-	-	-	-	-	0	-6.86	0
halon1211	1.0	0	0	0	0.16	1.0	1.0	1.0	0.897	0	0	0	4.45e-06	0.034	0	0.29	0
halon1211|o3	-	-	-	-	-	-	-	-	-	-	-	-	-	-	0	-3.33	0
halon1301	1.0	0	0	0	0.72	1.0	1.0	1.0	4.04	0	0	0	1e-15	0.0378	0	0.3	0
halon1301|o3	-	-	-	-	-	-	-	-	-	-	-	-	-	-	0	-1.64	0
halon2402	1.0	0	0	0	0.28	1.0	1.0	1.0	1.57	0	0	0	1e-15	0.0217	0	0.31	0
halon2402|o3	-	-	-	-	-	-	-	-	-	-	-	-	-	-	0	-6.76	0
hcfc141b	1.0	0	0	0	0.094	1.0	1.0	1.0	0.527	0	0	0	1e-15	0.0481	0	0.16	0
hcfc141b|o3	-	-	-	-	-	-	-	-	-	-	-	-	-	-	0	-0.0774	0
hcfc142b	1.0	0	0	0	0.18	1.0	1.0	1.0	1.01	0	0	0	1e-15	0.056	0	0.19	0
hcfc142b|o3	-	-	-	-	-	-	-	-	-	-	-	-	-	-	0	-0.0193	0
hcfc22	1.0	0	0	0	0.119	1.0	1.0	1.0	0.667	0	0	0	1e-15	0.0651	0	0.21	0
hcfc22|o3	-	-	-	-	-	-	-	-	-	-	-	-	-	-	0	-0.0171	0
hfc125	1.0	0	0	0	0.3	1.0	1.0	1.0	1.68	0	0	0	1e-15	0.0469	0	0.23	0
hfc134a	1.0	0	0	0	0.14	1.0	1.0	1.0	0.785	0	0	0	1e-15	0.0551	0	0.16	0
hfc143a	1.0	0	0	0	0.51	1.0	1.0	1.0	2.86	0	0	0	1e-15	0.067	0	0.16	0
hfc152a	1.0	0	0	0	0.016	1.0	1.0	1.0	0.0897	0	0	0	1e-15	0.0852	0	0.1	0
hfc227ea	1.0	0	0	0	0.36	1.0	1.0	1.0	2.02	0	0	0	1e-15	0.0331	0	0.26	0
hfc23	1.0	0	0	0	2.28	1.0	1.0	1.0	12.8	0	0	0	1e-15	0.0804	0	0.18	0
hfc236fa	1.0	0	0	0	2.13	1.0	1.0	1.0	11.9	0	0	0	1e-15	0.037	0	0.24	0
hfc245fa	1.0	0	0	0	0.079	1.0	1.0	1.0	0.443	0	0	0	1e-15	0.042	0	0.24	0
hfc32	1.0	0	0	0	0.054	1.0	1.0	1.0	0.303	0	0	0	1e-15	0.108	0	0.11	0
hfc365mfc	1.0	0	0	0	0.089	1.0	1.0	1.0	0.499	0	0	0	1e-15	0.038	0	0.22	0
hfc4310mee	1.0	0	0	0	0.17	1.0	1.0	1.0	0.953	0	0	0	1e-15	0.0223	0	0.359	0
methane	1.0	0	0	0	8.25	1.0	1.0	1.0	8.25	0	-0.3	0.00032	720	0.352	0	0	0.038
methane|o3	-	-	-	-	-	-	-	-	-	-	-	-	-	-	0	0.000163	0
methane|strat_h2o	-	-	-	-	-	-	-	-	-	-	-	-	-	-	0	4.37e-05	0
methyl_bromide	1.0	0	0	0	0.008	1.0	1.0	1.0	0.0448	0	0	0	0.0053	0.0593	0	0.004	0
methyl_bromide|o3	-	-	-	-	-	-	-	-	-	-	-	-	-	-	0	-3.07	0
methyl_chloride	1.0	0	0	0	0.009	1.0	1.0	1.0	0.0504	0	0	0	0.457	0.111	0	0.004	0
methyl_chloride|o3	-	-	-	-	-	-	-	-	-	-	-	-	-	-	0	-0.0501	0
nf3	1.0	0	0	0	5.69	1.0	1.0	1.0	31.9	0	0	0	1e-15	0.0792	0	0.2	0
nh3	1.0	0	0	0	1.0	1.0	1.0	1.0	1.0	0	0	0	1e-15	1.0	0	0	0
nitrous_oxide	1.0	0	0	0	100.0	1.0	1.0	1.0	63.2	0	0	0	270	0.201	0	0	0.106
nitrous_oxide|o3	-	-	-	-	-	-	-	-	-	-	-	-	-	-	0	0.000663	0
nmvoc	1.0	0	0	0	1.0	1.0	1.0	1.0	1.0	0	0	0	1e-15	1.0	0	0	0
nmvoc|o3	-	-	-	-	-	-	-	-	-	-	-	-	-	-	0	0.000308	0
nox	1.0	0	0	0	1.0	1.0	1.0	1.0	1.0	0	0	0	1e-15	1.0	0	0	0
nox_avi	1.0	0	0	0	1.0	1.0	1.0	1.0	1.0	0	0	0	1e-15	1.0	0	0	0
nox_avi|contrails	-	-	-	-	-	-	-	-	-	-	-	-	-	-	0	0.0164	0
nox|o3	-	-	-	-	-	-	-	-	-	-	-	-	-	-	0	0.00168	0
oc	1.0	0	0	0	1.0	1.0	1.0	1.0	1.0	0	0	0	1e-15	1.0	0	-0.0176	0
oc|aci	-	-	-	-	-	-	-	-	-	-	-	-	-	-	0	-0.00801	0
sf6	1.0	0	0	0	32.0	1.0	1.0	1.0	151	0	0	0	1e-15	0.0385	0	0.57	0
so2	1.0	0	0	0	1.0	1.0	1.0	1.0	1.0	0	0	0	171	1.0	0	-0.00474	0
so2f2	1.0	0	0	0	0.36	1.0	1.0	1.0	2.02	0	0	0	1e-15	0.0551	0	0.2	0
so2|aci	-	-	-	-	-	-	-	-	-	-	-	-	-	-	-0.956	0	0

Table S3. GWP metric for default parameter values computed against a baseline emission scenario that reproduces historical concentrations (Meinshausen et al., 2017) up to 2014, and fixed at the 2014 level thereafter. These are calculated using the total change in ERF arising from a 1 t emission pulse of each emission type in 2015.

timescale / years **agent**	5	10	20	50	100	500
bc	7530	4280	2420	1130	646	185
c2f6	7020	7570	8290	9390	10300	12200
c3f8	5770	6210	6800	7660	8360	9390
c4f10	5860	6310	6900	7780	8490	9530
c5f12	5520	5940	6510	7350	8050	9280
c6f14	5040	5430	5940	6710	7330	8330
c7f16	4990	5380	5880	6640	7250	8220
c8f18	4870	5240	5730	6470	7070	8010
c_c4f8	6200	6680	7310	8240	9020	10300
carbon_dioxide	1.0	1.0	1.0	1.0	1.0	1.0
carbon_tetrachloride	-1870	-1880	-1780	-1380	-936	-267
cf4	3970	4280	4680	5310	5850	7030
cfc11	2670	2740	2740	2420	1860	582
cfc113	3970	4170	4340	4230	3720	1460
cfc114	6270	6670	7120	7490	7310	4160
cfc115	4800	5150	5590	6170	6500	5690
cfc12	8290	8720	9110	9010	8040	3310
ch2cl2	115	65.0	36.7	17.2	9.82	2.82
ch3ccl3	-2430	-1810	-1140	-545	-310	-87.6
chcl3	208	117	66.3	31.2	17.8	5.1
co	18.1	10.3	5.81	2.73	1.55	0.444
halon1202	-48800	-30200	-16900	-7280	-3590	-54.1
halon1211	-59900	-55700	-46600	-28000	-15800	-3050
halon1301	-33300	-34600	-35300	-32800	-27000	-8660
halon2402	-87000	-85900	-79600	-58200	-37100	-8380
hcfc141b	2070	1780	1320	691	394	110
hcfc142b	5670	5380	4650	2980	1790	497
hcfc22	6920	6200	4880	2730	1570	438
hfc125	6790	6760	6370	4850	3230	913
hfc134a	5020	4610	3780	2220	1290	360
hfc143a	7000	7190	7190	6300	4820	1500
hfc152a	1650	966	546	256	146	41.7
hfc227ea	5500	5540	5340	4290	3000	867
hfc23	9850	10500	11300	12000	11900	7460
hfc236fa	6040	6440	6900	7310	7230	4370
hfc245fa	4990	4140	2930	1480	841	236
hfc32	5130	3900	2510	1200	682	193
hfc365mfc	4290	3650	2670	1380	785	220
hfc4310mee	4720	4440	3800	2390	1420	394
methane	119	99.4	71.3	36.3	20.6	5.79
methyl_bromide	-17900	-9940	-5360	-2180	-948	247
methyl_chloride	-578	-328	-185	-87.1	-49.6	-14.2
nf3	10900	11700	12700	14000	14800	13100
nh3	0	0	0	0	0	0
nitrous_oxide	308	324	338	334	297	121
nmvoc	38.5	21.9	12.4	5.8	3.3	0.946
nox	210	119	67.4	31.6	18.0	5.16
nox_avi	2050	1160	658	309	176	50.4
oc	-3210	-1820	-1030	-483	-275	-78.9
sf6	15100	16300	17800	20100	21900	24500
so2	-1280	-728	-411	-193	-110	-31.5
so2f2	7050	7110	6850	5500	3840	1110

S2 Radiative forcing of carbon dioxide, methane and nitrous oxide

Here we compare the concentration-forcing relationships of CO_2, CH_4 and N_2O used in FaIRv2.0.0, which exclude the interaction terms between gases, to the standard simple formulae detailed in Etminan et al. (2016). Figure S1 shows a comparison of the Oslo line-by-line (OLBL) data from Etminan et al. to both the Etminan et al. formulae and those used in FaIRv2.0.0. The main difference between the relationships used in FaIRv2.0.0 and those in Etminan et al. is the variance in the error when compared to the OLBL. The FaIRv2.0.0 relationships have a larger error variance at each CO_2 concentration than the Etminan et al. formulae (Figure S1). This is due to the lack of interaction terms, and results in a maximum absolute error of 0.115 W m^{-2} at concentrations of $CO_2 = 2000$ ppm, $CH_4 = 3500$ ppm, and $N_2O = 525$ ppm (the green triangle in the far right-hand side subplot in Figure S1). We believe that in the context of other uncertainties associated with such a high concentration scenario this error is defensible. We note (as was done in Etminan et al.) that the absolute uncertainty in the OLBL calculation is estimated to be 10% for CO_2 and N_2O and 14% for CH_4.

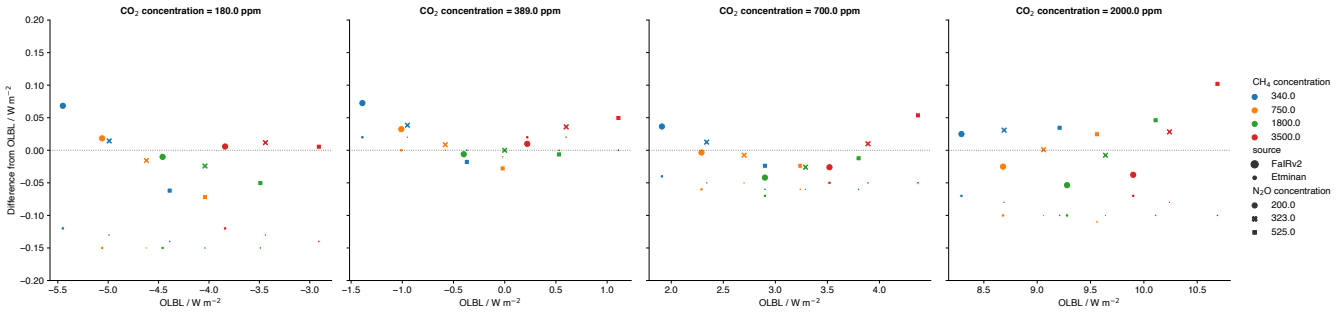

Figure S1. Comparison of the CO_2, CH_4 and N_2O ERF relationships used in FaIRv2.0.0 to the simple formulae and OLBL data from (Etminan et al., 2016). We show absolute differences from OLBL approach, grouped by CO_2 concentration. Marker size indicates source (Etminan et al. or FaIRv2.0.0-alpha), colour indicates CH_4 concentration, and style indicates N_2O concentration.

S3 Methane lifetime model

Here we illustrate the impact of including an interactive methane lifetime in FaIRv2.0.0. Running RCP8.5 (Riahi et al., 2011) through FaIRv2.0.0-alpha, the evolution of methane lifetime over history and through 2100 is shown in Figure S2. The simulated methane lifetime in 2010 is 8.90 years, compared to 9.15 years in Holmes et al. (2013); and the change in lifetime between 2010 and 2100 is 10.8 % compared to 10.3 %.

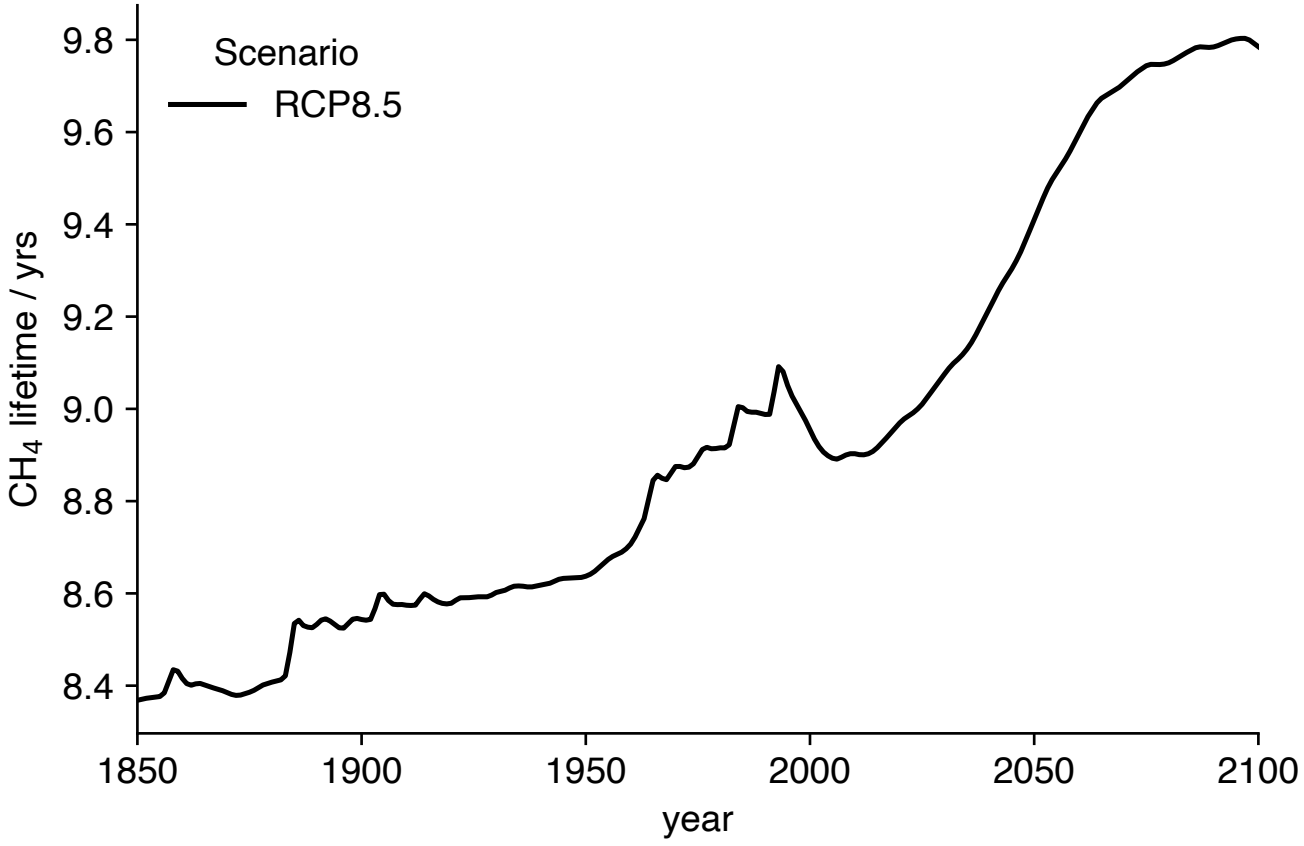

Figure S2. Evolution of the methane lifetime in FaIRv2.0.0-alpha under historical concentrations (Meinshausen et al., 2011) to 2005 and the RCP8.5 scenario thereafter.

S4 Non-linearities

Non-linearities in FaIRv2.0.0 arise primarily from the atmospheric decay feedbacks within the carbon and methane cycles (ie. from the state-dependent adjustment factor, $\alpha(t)$). All other non-linearities are due to forcing agents with non-zero f_1 or f_3 parameters. Here we attempt to understand and characterise the non-linearities within FaIRv2.0.0 using a set of pulse-response experiments. We use pulse-response experiments as even in a simple model such as FaIRv2.0.0, the existing gas-cycle and forcing non-linearities can result in relatively complex behaviour. Using SSP2-45 as the reference scenario, we add in emission pulses at the present-day (2019) over several orders of magnitude (0.01 to 1000 $GtCO_2$-eq) to the input carbon dioxide and methane emission timeseries in turn. The results of these experiments are shown in Figure S3. In the next paragraph, we step through how to understand these results, but a key message to emphasize is that these non-linearities are not very significant on the whole, and especially on longer (centennial) timescales.

In terms of characterisation, we will step through each variable in turn, explaining the processes behind their behaviour. Throughout this section, we refer to the difference between the experiments and the reference as the *anomaly*. In Figure S3, these are normalised by 1/(pulse size). We refer to the difference between the experimental anomalies relative to the smallest pulse experiment, normalised by 1/(pulse size) as the *non-linearity anomaly*; if the model were linear, the non-linearity anomalies would be zero. For the CO_2 pulse experiments:

- α_{CH_4} (and hence the CH_4 lifetime) is reduced by a CO_2 pulse due to the overall increase in temperature. The non-linearity anomalies increase as the pulse size increases, mirorring the non-linearity anomalies in temperature.
- α_{CO_2} is increased by a CO_2 pulse due to the increased CO_2 uptake and temperature. The non-linearity anomalies increase as the pulse size increases.
- CH_4 concentrations are reduced by a CO_2 pulse due to the reduction in CH_4 lifetime. The non-linearity anomalies increase (ie. the overall anomaly becomes less negative) as the pulse size increases.
- CO_2 concentrations are increased by a CO_2 pulse due to the increase in α_{CO_2}. The non-linearity anomalies increase as the pulse size increases, hence CO_2 concentrations are super-linear with emissions. However, the magnitude of the differences due to non-linearities are still small: < 0.5 ppm for pulses lower than 100 $GtCO_2$.
- CH_4 forcing anomalies and non-linearity anomalies follow the same behaviour as CH_4 concentrations.
- CO_2 forcing anomalies follow the same behaviour as CH_4 concentration anomalies. However, the non-linearity anomalies display different behaviour. Since CO_2 forcing is sub-linear with concentrations, the non-linearity anomaly is lower the larger the pulse size (the concentration-forcing sub-linearity dominates the emission-concentration super-linearity).
- Temperature anomalies are, as expected, positive for a CO_2 pulse. However, temperature non-linearity anomalies follow the same behaviour as CO_2 forcing, and are therefore sub-linear with CO_2 emissions. We note that the magnitude of the differences arising due to model non-linearity are < 0.005 K on all timescales, and < 0.001 K on centennial timescales for pulse sizes of < 100 $GtCO_2$.

The CH_2 pulse experiments can be analysed in an identical fashion. An additional feature of the behaviour during these experiments is that the sub-linearity of CH_4 forcing with concentrations dominates on very short timescales (meaning that the initial temperature non-linearity anomaly is negative), but for timescales of > 10 years, the super-linearity of CH_4 concentrations with emissions dominates; resulting in an overall long-term super-linear temperature response with CH_4 emissions. Note that even for emission pulses of CH_4, centennial non-linearities are driven by the carbon-cycle due to the short atmospheric lifetime of CH_4. However, we again stress that the overall differences arising due to model non-linearity are < 0.05 K on all timescales, and < 0.001 K on centennial timescales for pulse sizes of < 100 $GtCO_2$-eq.

Overall, the non-linearities appear insignificant for pulses of less than 10 $GtCO_2$-eq. It is important to note that for realstic emission scenarios these non-linearities would grow over time, so over long time periods non-linearities may be important even if the emission rates are significantly lower than 10 $GtCO_2$-eq.

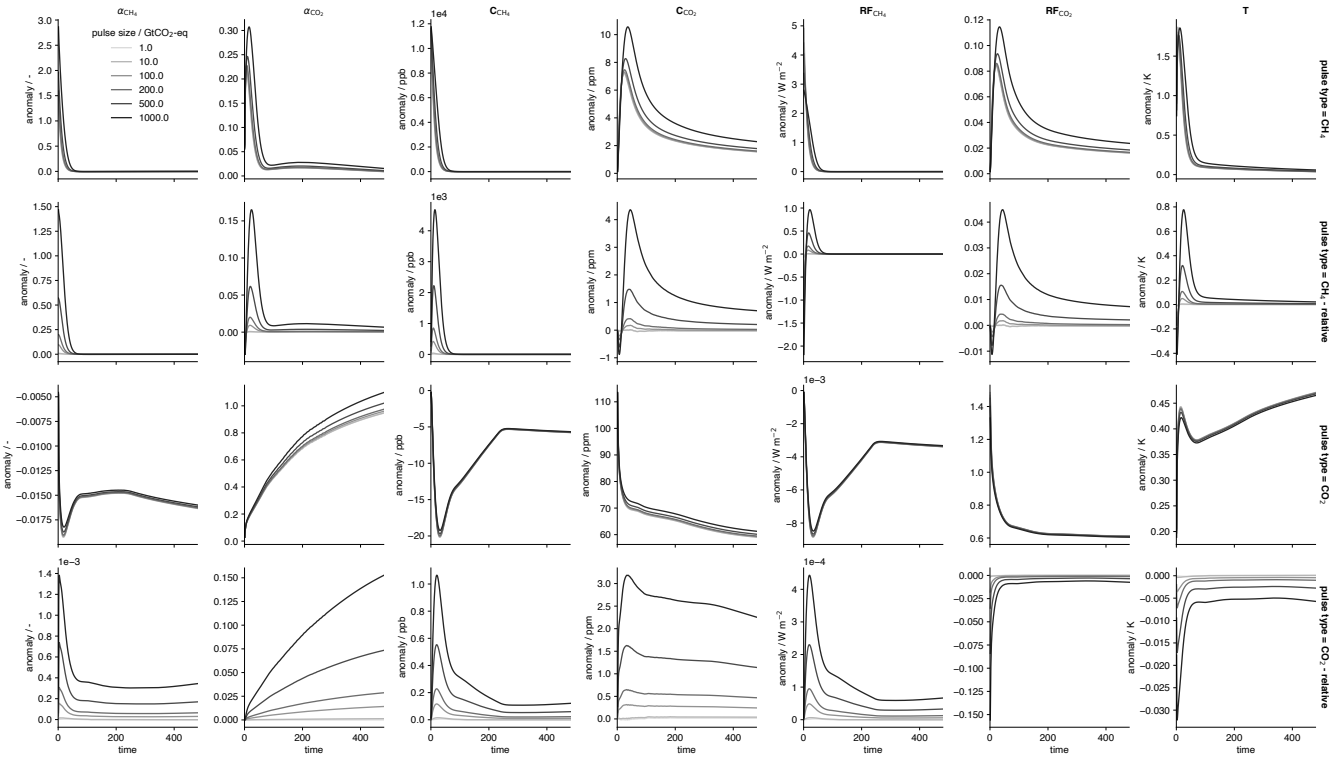

Figure S3. Demonstration of non-linear behaviour in FaIRv2.0.0 using pulse emission experiments. Top two rows show results from CO_2 pulse experiments, and bottom two show results from CH_4 experiments. The columns show, in order: CH_4 lifetime adjustment factor, CO_2 lifetime adjustment factor, CH_4 concentrations, CO_2 concentrations, CH_4 forcing, CO_2 forcing, and temperature response. Rows 1 and 3 show anomalies with respect to the reference (no pulse) experiment, scaled by 1/(pulse size). Rows 2 and 4 (marked as "relative") show the scaled anomalies relative to the anomaly for a pulse of size 0.01 $GtCO_2$-eq. The ratio of rows 1 and 2 (or 3 and 4) gives the fractional contribution of the nonlinearity relative to the size of the anomaly for each experiment. Non-linearities are not visible at these scales for pulses of less than 1 $GtCO_2$-eq.

S5 CMIP6 data pre-processing

CMIP6 data throughout this study is pre-processed as described in Nicholls et al. (2021), using a 21-year-running mean in the piControl experiment to normalise the data and calculate anomalies. The number of ensemble members per model for each experiment is given below in Table S4.

Table S4. Number of ensemble members per CMIP6 model in the idealised experiments used to tune the FaIRv2.0.0-alpha climate response in Section 3.1; and in the SSPs displayed in Figure 10.

experiment **model**	1pctCO2	abrupt-0p5xCO2	abrupt-2xCO2	abrupt-4xCO2	ssp119	ssp126	ssp245	ssp370	ssp460	ssp585
ACCESS-CM2	1	0	0	1	0	3	3	3	0	3
ACCESS-ESM1-5	1	0	0	1	0	3	3	3	0	3
AWI-CM-1-1-MR	1	0	0	1	0	1	1	5	0	1
BCC-CSM2-MR	1	0	0	1	0	1	1	1	0	1
BCC-ESM1	1	0	0	1	0	0	0	0	0	0
CAMS-CSM1-0	2	0	0	2	2	2	2	2	0	2
CESM2	1	1	1	0	0	3	6	3	0	5
CESM2-FV2	1	0	0	1	0	0	0	0	0	0
CESM2-WACCM	1	0	0	1	0	1	5	1	0	5
CESM2-WACCM-FV2	1	0	0	1	0	0	0	0	0	0
CMCC-CM2-SR5	1	0	0	1	0	1	1	1	0	1
CNRM-CM6-1	1	1	1	1	0	6	6	6	0	6
CNRM-CM6-1-HR	1	0	0	1	0	1	1	1	0	1
CNRM-ESM2-1	1	0	0	2	5	4	5	5	5	5
CanESM5	6	0	0	2	50	50	50	50	5	50
CanESM5-CanOE	1	0	0	0	0	3	3	3	0	3
E3SM-1-0	1	0	0	1	0	0	0	0	0	0
FGOALS-g3	3	0	0	1	1	4	4	5	1	4
GISS-E2-1-G	3	1	4	5	2	7	20	18	6	3
GISS-E2-1-H	1	0	1	2	0	0	0	0	0	0
GISS-E2-2-G	1	0	1	1	0	0	0	0	0	0
HadGEM3-GC31-LL	4	1	0	1	0	1	1	0	0	4
HadGEM3-GC31-MM	1	0	0	1	0	1	0	0	0	3
MIROC-ES2L	1	0	0	1	3	3	1	1	0	1
MIROC6	1	1	1	1	1	42	3	3	1	49
MPI-ESM-1-2-HAM	1	0	0	0	0	0	0	0	0	0
MPI-ESM1-2-HR	1	0	0	1	0	2	2	10	0	2
MPI-ESM1-2-LR	1	0	0	1	0	10	10	10	0	10
MRI-ESM2-0	2	1	1	6	1	1	1	5	1	2
NorCPM1	1	0	0	1	0	0	0	0	0	0
SAM0-UNICON	1	0	0	1	0	0	0	0	0	0
CIESM	0	0	0	0	0	1	1	0	0	1
EC-Earth3	0	0	0	0	51	7	22	6	0	57
EC-Earth3-Veg	0	0	0	0	3	5	6	4	0	5
FGOALS-f3-L	0	0	0	0	0	1	1	1	0	1
INM-CM4-8	0	0	0	0	0	0	0	0	0	1
INM-CM5-0	0	0	0	0	0	0	0	0	0	1
IPSL-CM6A-LR	0	0	0	0	6	6	11	11	7	6
KACE-1-0-G	0	0	0	0	0	3	3	3	0	3
KIOST-ESM	0	0	0	0	0	0	0	0	0	1
NESM3	0	0	0	0	0	2	2	0	0	2
NorESM2-LM	0	0	0	0	0	1	3	1	0	1
NorESM2-MM	0	0	0	0	0	1	1	1	0	1
TaiESM1	0	0	0	0	0	0	0	0	0	1
UKESM1-0-LL	0	0	0	0	5	13	6	13	0	5
Total models	31	6	7	28	12	32	31	28	7	36

S6 Energy balance model parameters

Using the method described in Cummins et al. (2020), we tune parameters to CMIP6 models for a 3-box version of the energy balance model described in Geoffroy et al. (2013), with the ocean heat uptake efficacy factor as Winton et al. (2010) included.

Table S5. CMIP6 tuned 3-box energy balance model. Nomenclature as Cummins et al. (2020).

parameter **model**	C_1	C_2	C_3	κ_1	κ_2	κ_3	ϵ	$F_{4\times CO_2}$
ACCESS-CM2	3.67	10.1	79.1	0.704	3.79	0.697	1.44	7.58
ACCESS-ESM1-5	5.08	33.7	272000000	1.15	0.957	0.261	1.24e-05	6.71
AWI-CM-1-1-MR	4.2	9.59	47.2	1.19	2.0	0.72	1.4	7.93
BCC-CSM2-MR	4.19	13.4	61.9	1.21	2.45	0.997	1.74	8.02
BCC-ESM1	5.22	19.9	87.5	0.82	1.3	0.721	1.17	5.76
CAMS-CSM1-0	4.33	8.06	53.9	1.86	3.96	0.667	1.2	8.72
CESM2-FV2	3.73	6.59	88.1	0.557	4.03	0.998	1.74	7.45
CESM2-WACCM	3.87	6.09	87.4	0.716	6.75	0.818	1.55	7.94
CESM2-WACCM-FV2	3.45	9.26	108	0.563	3.65	0.908	1.45	6.62
CMCC-CM2-SR5	4.33	18.5	138000	1.42	1.24	0.243	0.00876	8.3
CNRM-CM6-1	5.06	14.5	298	1.31	1.26	0.396	2.33e-05	8.66
CNRM-CM6-1-HR	5.47	13.3	106	1.11	1.61	0.541	0.563	8.25
CNRM-ESM2-1	4.31	6.56	99.6	0.645	2.51	0.726	0.873	5.79
CanESM5	4.13	10.5	72.5	0.622	2.04	0.63	1.04	7.19
E3SM-1-0	3.68	9.63	42.4	0.581	2.38	0.374	1.57	7.11
FGOALS-g3	4.29	8.6	92.3	1.25	2.54	1.01	1.28	7.67
GISS-E2-1-G	2.15	5.8	342	2.01	1.73	0.622	0.441	9.12
GISS-E2-1-H	4.32	23.2	7250000	1.48	1.3	0.327	0.258	7.67
GISS-E2-2-G	4.01	11.0	276	2.28	1.96	0.567	0.105	8.55
HadGEM3-GC31-LL	3.82	8.86	66.1	0.63	3.15	0.645	1.22	7.45
HadGEM3-GC31-MM	3.92	12.7	64.5	0.69	2.51	0.671	1.1	7.58
MIROC-ES2L	4.33	12.6	1760	2.32	1.97	0.517	7.43e-05	9.34
MIROC6	3.68	34.3	36100000	2.17	1.06	0.39	0.0458	9.1
MPI-ESM1-2-HR	6.12	34.0	211000000	1.72	1.03	0.25	3.98e-05	8.6
MPI-ESM1-2-LR	5.78	11.6	98.3	1.57	2.4	0.945	1.39	9.94
MRI-ESM2-0	3.66	9.97	99.9	0.863	2.37	1.07	0.942	5.76
NorCPM1	6.5	16.5	91.5	1.13	2.42	1.21	1.58	7.79
SAM0-UNICON	4.59	6.24	110	1.03	2.62	1.02	1.23	8.26

S7 Global Warming Index calculation

The Global Warming Index follows the methodology in Haustein et al. (2016), but updates several components. We carry out the calculation using 6 observational warming products (Lenssen et al., 2019; Cowtan and Way, 2014; Vose et al., 2012; Morice et al., 2011; Rohde et al., 2013; Morice et al., 2020), incorporating observational uncertainty either through the provided ensemble product, or if none exists, through the HadCRUT5 ensemble errors. We then generate 5000 realisations of historical ERF as follows. For all forcings excluding aerosol forcing, we take the best-estimate historical timeseries from Smith (2020), and scale them by factors drawn from the distributions detailed in table 6. For aerosol forcing, we take the best-estimate historical timeseries of ERFaci and ERFari, and scale them by scaling factors drawn from a skew-normal distribution that matches the quantiles of the constrained ERFaci and ERFari distributions stated in table 4 of Smith et al. (2020). We consider 18 different response model parameterisations, spanning the ranges of possible realised warming fraction (Millar et al., 2015) and response timescale (Geoffroy et al., 2013). Finally, we include uncertainty due to internal variability through timeseries from the piControl experiment of different CMIP6 models, rejecting models with a too large drift (here "too large" is $> \pm 0.15$ K / century); resulting in 102 different representations of internal variability (two random samples per model). Combining these sources of uncertainty gives a 1,836,000,000 member ensemble of the global warming index. For each observational product, we then randomly subsample 500,000,000 members which are used to estimate the distribution of the current level and rate of anthropogenic warming, and thus the FULL ensemble selection probabilities.

S8 Alternate baseline warming projections

Table S6. Projections of future warming as Table 10, but relative to a pre-industrial baseline period of 1850-1900 for comparison with Tokarska et al. (2020); Ribes et al. (2021). Shown are end of century warming (2081-2100), 2100 warming, and peak warming.

	percentile	5%	16.6%	50%	83.3%	95%
2081-2100 warming relative to 1850-1900 / K	**ssp119**	0.99	1.16	1.44	1.83	2.21
	ssp126	1.28	1.48	1.82	2.29	2.70
	ssp245	1.99	2.26	2.72	3.30	3.79
	ssp370	2.80	3.13	3.64	4.26	4.78
	ssp370-lowNTCF-aerchemmip	2.83	3.20	3.80	4.56	5.18
	ssp370-lowNTCF-gidden	2.42	2.75	3.29	3.96	4.51
	ssp434	1.56	1.77	2.14	2.61	3.04
	ssp460	2.28	2.58	3.05	3.65	4.15
	ssp534-over	1.55	1.79	2.21	2.78	3.30
	ssp585	3.31	3.74	4.44	5.31	6.03
2100 warming relative to 1850-1900 / K	**ssp119**	0.94	1.11	1.39	1.80	2.20
	ssp126	1.23	1.43	1.78	2.27	2.72
	ssp245	2.03	2.32	2.81	3.44	3.99
	ssp370	3.05	3.41	4.00	4.71	5.31
	ssp370-lowNTCF-aerchemmip	3.07	3.48	4.15	5.01	5.72
	ssp370-lowNTCF-gidden	2.63	2.99	3.60	4.36	4.99
	ssp434	1.52	1.74	2.11	2.61	3.08
	ssp460	2.35	2.66	3.18	3.84	4.41
	ssp534-over	1.44	1.68	2.10	2.68	3.24
	ssp585	3.57	4.05	4.84	5.84	6.66
peak warming relative to 1850-1900 / K	**ssp119**	1.25	1.39	1.64	1.96	2.28
	ssp126	1.39	1.58	1.90	2.33	2.75
	ssp534-over	1.89	2.14	2.55	3.05	3.50

S9 Short note on Implementation of FaIRv2.0.0

In this section, we outline the details of how we have implemented the development version of the FaIRv2.0.0 model (FaIRv2.0.0-alpha) in python. We note that these notes may not be relevant for all programming languages, but hope that they are useful regardless, especially where a forward difference timestepping scheme is used.

In our implementation, we use a forward difference scheme, in which output variables are assumed to be intra-timestep averages, and auxiliary variables (such as R or G_a) are calculated instantaneously at the start of each timestep. Within each timestep, we carry out the following sequence of computations:

1. Calculate $\alpha(t)$ using equation 3 with variables values from the previous timestep.
2. Calculate $C(\bar{t})$ by
   (a) calculating $R_i(t) = E(t) * a_i * \alpha(t) * \tau_i * [1 - \exp(\Delta t/(\alpha(t) * \tau_i))]/\Delta t + R(t-1) * \exp(\Delta t/(\alpha(t) * \tau_i))$
   (b) $G_a = \sum_{i=1}^{n} R_i(t)$
   (c) $C(\bar{t}) = C_0 + [G_a(t) + G_a(t-1)]/2$
3. Calculate $F(\bar{t})$ using equation 4.
4. Calculate $T(\bar{t})$ by
   (a) $S_j(t) = q_j * F(\bar{t}) * [1 - \exp(-\Delta t/d_i)] + S_j(t-1) * \exp(-\Delta t/d_i)$
   (b) $T(\bar{t}) = \sum_{j=1}^{3} [S_j(t-1) + S_j(t)]/2$
5. All output variables have now been computed, and the process restarts.

For clarity, we also provide a schematic, Figure S4, indicating at which point in each timestep each variable is assumed to reside in our implementation. In addition to our timestepping scheme, the other key feature of our implementation (and important property of FaIRv2.0.0) is that it is fully vectorised. Variables are represented by - and computations run over - multi-dimensional arrays. In our implementation, these arrays have dimensions for (where required): emission/ forcing scenario, gas/forcing parameter set, climate response parameter set, gas species, time, and any additional required dimensions (reservoirs for the carbon cycle or thermal boxes for the climate response). For example, the size of the array containing modelled concentrations in an emission driven run would be: S × P × C × G × t, where S is the number of scenarios, P the number of gas parameter sets, C the number of climate response sets, G the number of gas species and t the total number of timesteps. This ability of FaIRv2.0.0 to be vectorised significantly reduces computation time for array-focused languages such as Python or MatLab. However, an important point to note is that this "complete" vectorisation results in the stored variable arrays becoming large very rapidly (eg. a tenfold increase in each of the S, P and C dimensions would result in a thousandfold increase in the size of the stored arrays, and corresponding memory required). It is therefore important to check that the total size of the stored

arrays won't exceed the total size of the available memory on the machine. It is possible that we could implement some form of "lazy" computation to alleviate this issue, for example by using Dask[1], but we have not done so in the FaIRv2.0.0-alpha implementation accompanying this paper.

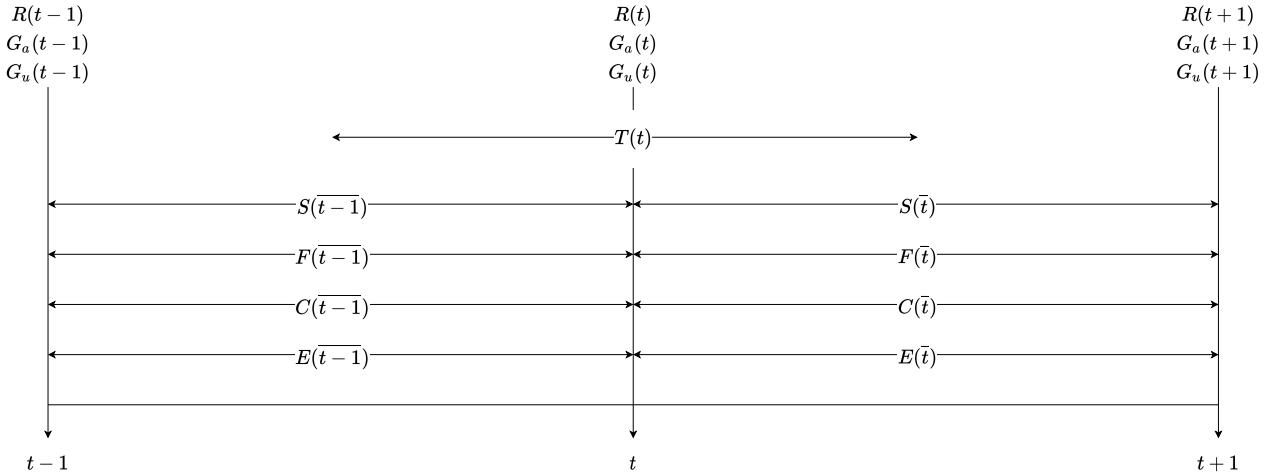

Figure S4. Variable residence within FaIRv2.0.0-alpha timestepping scheme.

[1]https://dask.org/

Code and data availability. The FaIRv2.0.0-alpha model code used in this study is publicly available at https://doi.org/10.5281/zenodo.4683173. The code and notebooks used to reproduce the analysis and figures is publicly available at https://doi.org/10.5281/zenodo.4683388. All data used in this study is publicly available at the relevant cited sources.

References

Cowtan, K. and Way, R. G.: Coverage bias in the HadCRUT4 temperature series and its impact on recent temperature trends, Quarterly Journal of the Royal Meteorological Society, 140, 1935–1944, https://doi.org/10.1002/qj.2297, 2014.

Cummins, D. P., Stephenson, D. B., and Stott, P. A.: Optimal estimation of stochastic energy balance model parameters, Journal of Climate, 33, 7909–7926, https://doi.org/10.1175/JCLI-D-19-0589.1, 2020.

Etminan, M., Myhre, G., Highwood, E. J., and Shine, K. P.: Radiative forcing of carbon dioxide, methane, and nitrous oxide: A significant revision of the methane radiative forcing, Geophysical Research Letters, 43, 12,614–12,623, https://doi.org/10.1002/2016GL071930, 2016.

Geoffroy, O., Saint-Martin, D., Olivié, D. J. L., Voldoire, A., Bellon, G., Tytéca, S., Geoffroy, O., Saint-Martin, D., Olivié, D. J. L., Voldoire, A., Bellon, G., and Tytéca, S.: Transient Climate Response in a Two-Layer Energy-Balance Model. Part I: Analytical Solution and Parameter Calibration Using CMIP5 AOGCM Experiments, Journal of Climate, 26, 1841–1857, https://doi.org/10.1175/JCLI-D-12-00195.1, 2013.

Haustein, K., L Otto, F. E., Uhe, P., Schaller, N., Allen, M. R., Hermanson, L., Christidis, N., McLean, P., and Cullen, H.: Real-time extreme weather event attribution with forecast seasonal SSTs, Environ. Res. Lett, 11, 64 006, https://doi.org/10.1088/1748-9326/11/6/064006, 2016.

Holmes, C. D., Prather, M. J., Søvde, O. A., and Myhre, G.: Future methane, hydroxyl, and their uncertainties: key climate and emission parameters for future predictions, Atmospheric Chemistry and Physics, 13, 285–302, https://doi.org/10.5194/acp-13-285-2013, 2013.

Lenssen, N. J. L., Schmidt, G. A., Hansen, J. E., Menne, M. J., Persin, A., Ruedy, R., and Zyss, D.: Improvements in the uncertainty model in the Goddard Institute for Space Studies Surface Temperature (GISTEMP) analysis, Journal of Geophysical Research: Atmospheres, p. 2018JD029522, https://doi.org/10.1029/2018JD029522, 2019.

Meinshausen, M., Smith, S. J., Calvin, K., Daniel, J. S., Kainuma, M. L. T., Lamarque, J.-F., Matsumoto, K., Montzka, S. A., Raper, S. C. B., Riahi, K., Thomson, A., Velders, G. J. M., and van Vuuren, D. P.: The RCP greenhouse gas concentrations and their extensions from 1765 to 2300, Climatic Change, 109, 213–241, https://doi.org/10.1007/s10584-011-0156-z, 2011.

Meinshausen, M., Vogel, E., Nauels, A., Lorbacher, K., Meinshausen, N., Etheridge, D. M., Fraser, P. J., Montzka, S. A., Rayner, P. J., Trudinger, C. M., Krummel, P. B., Beyerle, U., Canadell, J. G., Daniel, J. S., Enting, I. G., Law, R. M., Lunder, C. R., O'Doherty, S., Prinn, R. G., Reimann, S., Rubino, M., Velders, G. J. M., Vollmer, M. K., Wang, R. H. J., and Weiss, R.: Historical greenhouse gas concentrations for climate modelling (CMIP6), Geoscientific Model Development, 10, 2057–2116, https://doi.org/10.5194/gmd-10-2057-2017, 2017.

Millar, R. J., Otto, A., Forster, P. M., Lowe, J. A., Ingram, W. J., and Allen, M. R.: Model structure in observational constraints on transient climate response, Climatic Change, 131, 199–211, https://doi.org/10.1007/s10584-015-1384-4, 2015.

Morice, C. P., Kennedy, J. J., Rayner, N. A., Jones, P. D., P., M. C., J., K. J., A., R. N., and D., J. P.: Quantifying uncertainties in global and regional temperature change using an ensemble of observational estimates: The HadCRUT4 data set, Journal of Geophysical Research: Atmospheres, 117, https://doi.org/10.1029/2011JD017187, 2011.

Morice, C. P., Kennedy, J. J., Rayner, N. A., Winn, J. P., Hogan, E., Killick, R. E., Dunn, R. J. H., Osborn, T. J., Jones, P. D., and Simpson, I. R.: An updated assessment of near-surface temperature change from 1850: the HadCRUT5 dataset, Journal of Geophysical Research: Atmospheres, https://doi.org/10.1029/2019JD032361, 2020.

Nicholls, Z., Lewis, J., Makin, M., Nattala, U., Zhang, G. Z., Mutch, S. J., Tescari, E., and Meinshausen, M.: Regionally aggregated, stitched and de-drifted CMIP-climate data, processed with netCDF-SCM v2.0.0, Geoscience Data Journal, 00, gdj3.113, https://doi.org/10.1002/gdj3.113, 2021.

Riahi, K., Rao, S., Krey, V., Cho, C., Chirkov, V., Fischer, G., Kindermann, G., Nakicenovic, N., and Rafaj, P.: RCP 8.5—A scenario of comparatively high greenhouse gas emissions, Climatic Change, 109, 33–57, https://doi.org/10.1007/s10584-011-0149-y, 2011.

Ribes, A., Qasmi, S., and Gillett, N. P.: Making climate projections conditional on historical observations, Science Advances, 7, eabc0671, https://doi.org/10.1126/sciadv.abc0671, 2021.

Rohde, R., Muller, R. A., Jacobsen, R., Muller, E., Perlmutter, S., Rosenfeld, A., Wurtele, J., Groom, D., and Wickham, C.: A New Estimate of the Average Earth Surface Land Temperature Spanning 1753 to 2011, Geoinformatics & Geostatistics: An Overview, 1, 1, https://doi.org/10.4172/2327-4581.1000101, 2013.

Smith, C.: Effective Radiative Forcing Time Series from the Shared Socioeconomic Pathways, https://doi.org/10.5281/ZENODO.3973015, 2020.

Smith, C. J., Harris, G., Palmer, M. D., Bellouin, N., Myhre, G., Schulz, M., Golaz, J.-C., Ringer, M., Storelvmo, T., and Forster, P. M.: Energy Budget Constraints on the Time History of Aerosol Forcing and Climate Sensitivity, Journal of Geophysical Research: Atmospheres, in submiss, https://doi.org/10.1002/ESSOAR.10503977.2, 2020.

Tokarska, K. B., Stolpe, M. B., Sippel, S., Fischer, E. M., Smith, C. J., Lehner, F., and Knutti, R.: Past warming trend constrains future warming in CMIP6 models, Science Advances, 6, eaaz9549, https://doi.org/10.1126/sciadv.aaz9549, 2020.

Vose, R. S., Arndt, D., Banzon, V. F., Easterling, D. R., Gleason, B., Huang, B., Kearns, E., Lawrimore, J. H., Menne, M. J., Peterson, T. C., Reynolds, R. W., Smith, T. M., Williams, C. N., Wuertz, D. B., Vose, R. S., Arndt, D., Banzon, V. F., Easterling, D. R., Gleason, B., Huang, B., Kearns, E., Lawrimore, J. H., Menne, M. J., Peterson, T. C., Reynolds, R. W., Smith, T. M., Jr., C. N. W., and Wuertz, D. B.: NOAA's Merged Land–Ocean Surface Temperature Analysis, Bulletin of the American Meteorological Society, 93, 1677–1685, https://doi.org/10.1175/BAMS-D-11-00241.1, 2012.

Winton, M., Takahashi, K., and Held, I. M.: Importance of Ocean Heat Uptake Efficacy to Transient Climate Change, Journal of Climate, 23, 2333–2344, https://doi.org/10.1175/2009JCLI3139.1, 2010.